Formation of a New Buried Charge Drives a Large-Amplitude Protein Quake in Photoreceptor Activation†

Aihua Xie,*,‡ Lorand Kelemen,‡,§ Johnny Hendriks,|| Brandy J. White,‡ Klaas J. Hellingwerf,|| and Wouter D. Hoff⊥

Department of Physics, Oklahoma State University, 145 Physical Sciences II, Stillwater, Oklahoma 74078, Department of Microbiology, University of Amsterdam, Nieuwe Achtergracht 166, 1018 WS Amsterdam, The Netherlands, and Department of Biochemistry and Molecular Biology, The University of Chicago, Chicago, Illinois 60637

Received October 23, 2000; Revised Manuscript Received December 15, 2000

ABSTRACT: Photoactive yellow protein (PYP) is a eubacterial photoreceptor and a structural prototype of the PAS domain superfamily of receptor and regulatory proteins. We investigate the activation mechanism of PYP using time-resolved Fourier transform infrared (FTIR) spectroscopy. Our data provide structural, kinetic, and energetic evidence that the putative signaling state of PYP is formed during a large-amplitude protein quake that is driven by the formation of a new buried charge, COO^- of the conserved Glu46, in a highly hydrophobic pocket at the active site. A protein quake is a process consisting of global conformational changes that are triggered and driven by a local structural "fault". We show that large, global structural changes take place after Glu46 ionization via intramolecular proton transfer to the anionic *p*-coumarate chromophore, and are suppressed by the absence of COO^- formation in the E46Q mutant. Our results demonstrate the significance of buried charge formation in photoreceptor activation. This mechanism may serve as one of the general themes in activation of a range of receptor proteins. In addition, we report the results of time-resolved FTIR spectroscopy of PYP crystals. The direct comparison of time-resolved FTIR spectroscopic data of PYP in aqueous solution and in crystals reveals that the structure of the putative signaling state is not developed in $P6_3$ crystals. Therefore, when the structural developments during the functional process of a protein are experimentally determined to be very different in crystals and solutions, one must be cautious in drawing conclusions regarding the functional mechanism of proteins based on time-resolved X-ray crystallography.

Embedding a charged group inside a protein in a nonpolar (low-dielectric) environment is energetically unfavorable. Therefore, most charged groups in a protein are solvent-exposed. Buried charges are unique and generally well conserved, indicating their structural and functional importance. To lower the electrostatic energy for embedding a charged group inside a protein, a buried charge must be stabilized through a network of polar groups, hydrogen bonding, and salt bridge interactions (*1*). Buried charges are important in protein folding (*1*, *2*). During the functional process of a protein, proton transfer events may lead to the formation of a new buried charge. Such a relocation of a buried charge in a protein may demand a new protein conformation. Although there are many studies on proton transfer events in energy transduction, formation of a new buried charge in triggering large conformational changes in a protein has not received significant attention. Here we show that formation of a new buried charge drives a large-amplitude protein quake that leads to PYP[1] photoreceptor activation. A protein quake (*3*) is a process consisting of global conformational changes that are triggered and driven by a local structural "fault".

PYP is a structural prototype of the PAS domain superfamily (*4*, *5*) of receptor and regulatory proteins from all three kingdoms of life. As a small water soluble photoreceptor (*6*−*8*), PYP bears a unique thioester-linked *p*-coumaric acid (pCA) chromophore (*9*, *10*) for light detection. Photoexcitation of the initial receptor state, pG_{446} (peak absorption at 446 nm), leads to a photocycle (*6*, *11*, *12*) that involves at least two intermediate states, pR_{465} ($\lambda_{max} = 465$ nm) and pB_{355} ($\lambda_{max} = 355$ nm), from 5 ns until the completion of the PYP photocycle in a few seconds. The long-lived pB_{355} state is the putative signaling state of PYP.

To investigate the molecular mechanism of PYP photoreceptor activation, we have performed time-resolved Fourier

† This work was supported by ONR Grant N00014-98-1-0854 and OCAST Fund HR98-24 to A.X., grants from the American Cancer Society (IRG-41-40) and the Cancer Research Foundation (19428) to W.D.H., and grants from the Netherlands Organization for Scientific Research (330-031/D97) and the Netherlands Foundation for Chemical Research to K.J.H.

* To whom correspondence should be addressed. E-mail: aihua@westlake.phy.okstate.edu. Telephone: (405) 744-3416. Fax: (405) 744-6811.

‡ Oklahoma State University.

§ Present address: Biological Research Centre, Institute of Biophysics, Szeged H-6726, Hungary.

|| University of Amsterdam.

⊥ The University of Chicago.

[1] Abbreviations: PYP, photoactive yellow protein; pG_{446}, initial receptor state with peak absorption (λ_{max}) at 446 nm; pR_{465}, red-shifted photocycle intermediate with a λ_{max} of 465 nm; pB_{355}, blue-shifted photocycle intermediate with a λ_{max} of 355 nm; pCA, *p*-coumaric acid (4-hydroxycinnamic acid); FTIR, Fourier transform infrared; CaF_2, calcium fluoride; PAS, originated from signaling proteins of "PER" (periodic clock protein), "ARNT" (aryl hydrocarbon receptor nuclear translator), and "SIM" (single-minded protein); bR, bacteriorhodopsin.

10.1021/bi002449a CCC: $20.00
Published on Web 01/18/2001

transform infrared (FTIR) spectroscopic measurements of the infrared difference spectra between the photocycle intermediates and the receptor state from 10 μs to the completion of the PYP photocycle. We have identified five major spectral markers that are sensitive to crucial structural changes. These spectral markers are employed to probe the kinetics and the nature of structural transitions that result in PYP photoreceptor activation.

MATERIALS AND METHODS

Sample Preparation. Purified proteins of wild-type PYP (wt-PYP) and the E46Q mutant were obtained using the method previously reported (*13*). PYP samples for FTIR experiments were prepared with a protein concentration of approximately 10 mM in 100 mM potassium phosphate buffer in D_2O at pH* 7.0. This was achieved by dissolving about 3 mg of purified and freeze-dried PYP in 300 μL of the above buffer, and washing it three times through Microcon centrifuge filters at 14000*g*. Each solution sample was made by sandwiching 2.5 μL of the PYP solution between two CaF_2 plates 25 mm in diameter and 2 mm thick using a 12 μm spacer. The $P6_3$ PYP crystals were grown using the reported protocol (*14*). PYP crystal samples for FTIR experiments were made from polycrystals gently ground between two CaF_2 plates without a spacer. With polycrystals, the sample is effectively isotropic, so the detected signals are averaged over all crystal orientations. The kinetics of polycrystalline PYP samples were tested using time-resolved visible absorption spectroscopy, and were found to be faster than those in solution, in agreement with the reported kinetic measurement of PYP single $P6_3$ crystals using visible absorption spectroscopy (*15*).

Time-Resolved FTIR Spectroscopy. A Bruker IFS 66v FTIR spectrometer was utilized for time-resolved measurements in the spectral range of 1900−970 cm^{-1}. The PYP photocycle was triggered using laser pulses with a pulse duration of 4 ns and an energy of 6 mJ at 450 nm for wt-PYP and 430 nm for the E46Q mutant (Continuum Surelite-II pumped OPO laser). The laser repetition rate was 0.5 Hz. The laser beam size at the samples was 6 mm in diameter. The pR_{465} to pB_{355} transition in aqueous wt-PYP was probed from 10 μs to 7 ms using time-resolved step-scan FTIR spectroscopy with a time resolution of 10 μs and a spectral resolution of 4 cm^{-1}. The pB to pG transitions in aqueous wt-PYP, the E46Q mutant, and the $P6_3$ crystals of wt-PYP were monitored from 60 ms to 2 s using time-resolved rapid-scan FTIR spectroscopy with a time resolution of 60 ms and a spectral resolution of 4 cm^{-1}. The heating effect on PYP crystals was less than 2 K based on 90% absorption of laser pulse energy.

Data Analysis. All time-resolved FTIR difference spectra were calculated using the preflash data (pG_{446}) as a baseline, and averaged over repetitive measurements. The time-resolved step-scan FTIR spectra at 25 μs, 100 μs, 400 μs, 1.6 ms, and 6.6 ms (Figure 1A) were further averaged over 2, 4, 16, 64, and 256 time points, respectively, around the specified times. The kinetic data of each peak (Figure 1B) were averaged to a quasi-logarithmic base with four data points per doubling time. The $pB_{355} - pG_{446}$ spectra (Figure 3) of wt-PYP, the E46Q mutant, and PYP in $P6_3$ crystals were the first time slices (60 ms) of the corresponding time-resolved rapid-scan FTIR data sets. The FTIR difference spectra of pR_{465}, pB'_{355}, and pB_{355} [$\Delta A_{pR}(\nu) = A_{pR}(\nu) - A_{pG}(\nu)$, $\Delta A_{pB'}(\nu)$, and $\Delta A_{pB}(\nu)$] were extracted from the experimental data of time-resolved step-scan FTIR difference spectra, $\Delta A(t,\nu)$, using the equation $\Delta A(t,\nu) = p_{pR}(t)\Delta A_{pR}(\nu) + p_{pB'}(t)\Delta A_{pB'}(\nu) + p_{pB}(t)\Delta A_{pB}(\nu)$. The population accumulations of photocycle intermediates pR_{465}, pB'_{355}, and pB_{355} [$p_{pR}(t)$, $p_{pB'}(t)$, and $p_{pB}(t)$, respectively] were calculated on the basis of a unidirectional unbranched photocycle model ($pR_{465} \rightarrow pB'_{355} \rightarrow pB_{355} \rightarrow pG_{446}$) with time constants of 260 μs, 2.0 ms, and 350 ms, respectively. The extracted $pB_{355} - pG_{446}$ spectrum (Figure 1C) is found to be essentially identical to the one (Figure 3) directly obtained from time-resolved rapid-scan FTIR measurements at 60 ms following laser excitation, when only pB_{355} and pG_{446} are populated. This demonstrates the reliability of our spectral calculations described here.

Calculation of the Electrostatic Energy for a Buried Charge. The electrostatic energy U (*16*), which is stored in an electric field generated by a small charged group with a net charge q and a dipole moment p in a homogeneous spherical shell of a dielectric medium with an inner radius R and a thickness D, is

$$U = \frac{1}{8\pi\epsilon_0\epsilon}\left[q^2\left(\frac{1}{R} - \frac{1}{R+D}\right) + \frac{2p^2}{3}\left(\frac{1}{R^3} - \frac{1}{(R+D)^3}\right)\right]$$

where ϵ_0 (=8.85 $C^2\ N^{-1}\ m^{-2}$) is the permittivity of vacuum and ϵ is the dielectric constant. The prefactor ($1/4\pi\epsilon_0$) has a value of 14.4 eV, or 1524 kJ/mol. To the first order of approximation, this electrostatic energy due to a COO^- group in a dielectric medium is calculated using an R of 2.50 Å and a D of 4.00 Å for the first shell of atoms surrounding the COO^- group, based on the Glu46 in the PYP crystal structure. The value of D is obtained on the basis of the diameters of C and O atoms plus the effects of hydrogen atoms and the nonequal distances from the center of the COO^- group. The value of R is obtained from the average interatomic distances (4.5 Å) between the center of the COO^- group of Glu46 and the 13 neighboring atoms that form the first shell of the binding pocket (with $R + D/2 = 4.5$ Å) based on the crystal structure of pG_{446} (*14*). To calculate the electrostatic energy difference (ΔU) between the same charged group at two different binding sites in a protein, the contributions to ΔU from the first shells of atom that define the properties of the two binding pockets (e.g., hydrophilic and hydrophobic) are dominant, while the regions beyond the first shells contain many more atoms per shell and are much less different on average. As a result, their contributions to ΔU are small and not accounted for in our calculation.

RESULTS AND DISCUSSION

Time-resolved FTIR spectroscopy is a powerful technique that provides both excellent time resolution (*17*) and high structural sensitivity (*18*). We employed this technique to probe chromophore photoisomerization, proton transfer, and global conformational changes involving the protein backbone and environments of polar side chain groups during the PYP photocycle. The E46Q mutant was studied in an effort to clarify the role of buried charge formation in PYP

activation. In addition, time-resolved FTIR spectroscopy is applicable to proteins both in solutions and in crystals. We have examined the structural developments during the PYP photocycle in $P6_3$ crystals using time-resolved rapid-scan FTIR spectroscopy.

Time-resolved FTIR difference spectra between the photocycle intermediates and pG_{446} (Figure 1A) reveal progressive structural changes in PYP from 25 μs to 6.6 ms following photoexcitation. Positive bands arise from photocycle intermediates, whereas negative ones arise from pG_{446}. Only structurally active groups during the PYP photocycle are detected in the time-resolved FTIR difference spectra. Those structural groups that do not undergo any structural changes make no contribution to the difference spectra. We have identified five spectral markers for probing important structural changes during PYP activation. The 1726 cm^{-1} band is assigned to the COOD group of Glu46 (*13*). The bands at 1498 and 1514 cm^{-1} are attributed to the phenolic ring vibration of the ionized and neutral pCA chromophore, respectively (unpublished results). The positive band centered at 1624 cm^{-1} arises predominantly from the C═O stretching of the protein backbone (amide I) in antiparallel β-structure (*19*, *20*). The 1689 cm^{-1} band is due to a ND-containing side chain group (Arg, Asn, or Gln), based on its sensitivity to ^{15}N isotopic labeling and to H−D exchange (unpublished results). The region between 1610 and 1560 cm^{-1} is largely attributed to various polar side chain groups containing double bonds (*21*).

To resolve the temporal order and kinetics of key structural events during the pR_{465} to pB_{355} transition, we have analyzed the kinetics (Figure 1B) of chromophore protonation [(■) characteristic upshift of the pCA ring vibration from 1498 to 1514 cm^{-1}] (unpublished results), Glu46 ionization [(□) depletion of the 1726 cm^{-1} band] (*13*), protein conformational changes at amide I [(○) increase in the intensity of the 1624 cm^{-1} band] (*19*), and a side chain [(●) depletion of the 1689 cm^{-1} band] (unpublished results). We found that the pR_{465} to pB_{355} transition is biphasic. The fast phase (τ_1 = 260 μs) predominantly encompasses pCA protonation and Glu46 ionization, while the slow phase (τ_2 = 2 ms) primarily involves large conformational changes in PYP. The data unambiguously demonstrate that a new buried charge, COO^- of Glu46, is formed prior to large global conformational changes.

The biphasic kinetics of the pR_{465} to pB_{355} transition reveal a new photocycle intermediate, pB'_{355}. The pB'_{355} state serves as an important structural link between pR_{465} and pB_{355}, and is critical for understanding the mechanism of signaling state formation. The pB'_{355} − pG_{446} spectrum (Figure 1C) shows that in pB'_{355}, Glu46 is ionized (bleaching at 1728 cm^{-1}), the pCA is protonated (peak shift from 1498 to 1514 cm^{-1}), and the conformation of pB'_{355} strongly resembles that of pG_{446} (minimal changes in amide I and in side chain groups). The COOD group in pG_{446} is buried in a highly hydrophobic environment (Figure 2), confined by the rigid and nonpolar side chain groups of Ile31, Ile49, and Val122. Since the conformation of pB'_{355} closely resembles that of pG_{446} (Figure 1C) and the binding pocket of the COOD group of Glu46 in pG_{446} is very rigid, we therefore conclude that the newly formed charge, COO^- of Glu46, in pB'_{355} remains in its highly hydrophobic environment, and is energetically unstable.

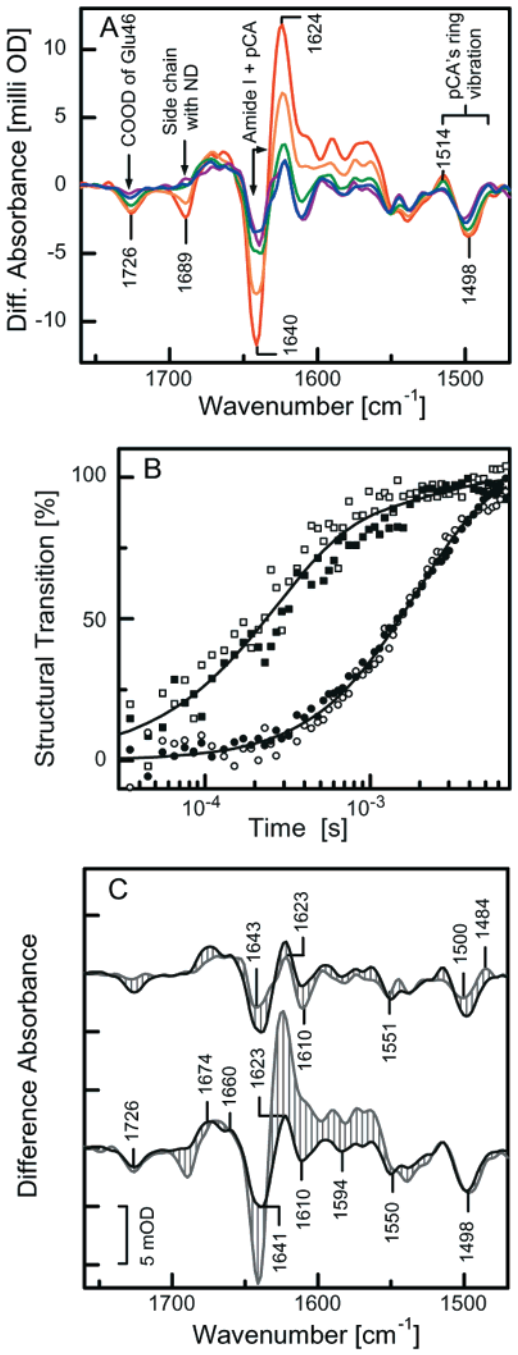

FIGURE 1: Time-resolved FTIR spectroscopy of the PYP photocycle. (A) Time-resolved FTIR difference spectra of wt-PYP at pH* 7 in D_2O at 25 μs (purple), 100 μs (blue), 400 μs (green), 1.6 ms (orange), and 6.6 ms (red). (B) The temporal courses of key structural events during the PYP photocycle: pCA protonation (■, 1498 cm^{-1}), Glu46 ionization (□, 1726 cm^{-1}), protein secondary structural changes (○, 1624 cm^{-1}), and dramatic changes in the environment of a ND-containing side chain (●, 1689 cm^{-1}). Nonlinear least-squares fitting (—) of the data to two-exponential kinetics yields a τ_1 of 260 μs and a τ_2 of 2.0 ms. The time constant for the fast kinetics is in agreement with the decay of pR from previous studies at neutral pH and room temperature (*6*, *11*). (C) Difference infrared spectra of pR_{465} (gray, top), pB'_{355} (black, top and bottom), and pB_{355} (gray, bottom) with respect to pG_{446}. The shaded areas represent the extent of structural changes during the pR_{465} to pB'_{355} transition (top) and the pB'_{355} to pB_{355} transition (bottom).

Glu46 Is the Proton Donor for Chromophore Protonation. In pG_{446}, the COOH group of Glu46 is hydrogen bonded to the negatively charged phenolic oxygen of the chromophore

(*13*, *14*). This hydrogen bond may be disrupted in pR_{465} due to chromophore photoisomerization. It was found that this bond is intact in pR_{465} at 80 K (FTIR difference spectroscopy) (*13*), but broken in pR_{465} at room temperature (nanosecond time-resolved X-ray crystallography) (*22*). This issue is crucial to understanding the proton transfer pathway for PYP activation.

Our time-resolved FTIR spectroscopic data of the PYP photocycle at room temperature unambiguously determine the hydrogen bonding status of Glu46 in pR_{465}. The COOD stretching frequency of Glu46 would be shifted from 1726 cm^{-1} in pG_{446} to approximately 1750 cm^{-1} upon loss of the hydrogen bond (*23*) or to $\leq$1600 cm^{-1} upon ionization (*21*). The $pR_{465} - pG_{446}$ spectrum (Figure 1C) reveals that (i) the carboxylic group of Glu46 remains protonated in pR_{465} (no depletion of the 1726 cm^{-1} band), (ii) the COOD group of Glu46 is unperturbed in pR_{465} (no significant peak shifts of the 1726 cm^{-1} band), and (iii) the protein conformation of pR_{465} remains unchanged from that of pG_{446} (a small peak at 1623 cm^{-1} arises from the chromophore due to photoisomerization, unpublished results). In addition, there is no alternative hydrogen bond partner for the COOD group of Glu46 within 4 Å (*14*). Therefore, the COOD group of Glu46 remains neutral and hydrogen bonded to the phenolic oxygen of the chromophore in pR_{465}.

Furthermore, pCA protonation and Glu46 ionization take place with identical kinetics (Figure 1B) with essentially no associated protein conformational changes (Figure 1C). We therefore conclude that a direct intramolecular proton transfer takes place from the COOD group of Glu46 to the negatively charged phenolic oxygen of the pCA chromophore during the pR_{465} to pB'_{355} transition.

It is intriguing that protonation of the chromophore in the E46Q mutant is 5 times faster than in wt-PYP at neutral pH (*24*). However, this does not provide informative evidence against the role of Glu46 as the proton donor for pCA in wt-PYP. First, the chromophore in the E46Q mutant may be protonated by direct proton transfer via a hydrogen-bonded wire (*25*) involving the OH groups of Tyr42 and Thr50, when the primary proton donor, COOH of Glu46, is absent. Second, the rate of this secondary protonation pathway may be increased due to an increased proton affinity of the chromophore caused by the E46Q mutation. It is important to point out that the electronic state of the pCA chromophore is perturbed by the E46Q mutation, as observed from changes in the peak positions and amplitudes of the chromophore vibration bands (Figure 3A) and a significant red shift of the visible peak absorption (*24*, *26*) from 446 nm in wt-PYP to 462 nm in the E46Q mutant. In addition, the faster protonation of the chromophore in the E46Q mutant can also be due to a reduced energy barrier for the pR to pB′ transition, since pB′ in the mutant is formed without creating a new buried charge at the hydrophobic binding site. Finally, our observation that the E46Q mutation greatly reduces the extent of structural changes during the formation of the pB-like state (see Figure 3 and below) fully supports the role of Glu46 as the proton donor in wt-PYP and its importance in PYP activation.

Formation of a New Buried Charge, COO^- of Glu46, Drives Large Conformational Changes. Extensive evidence showing that the protein conformation of the putative signaling state, pB_{355}, is largely different from that of pG_{446} has been reported (*27*, *28*). Comparison of the infrared difference spectra of pR_{465}, pB'_{355}, and pB_{355} (Figure 1C) reveals that such large conformational changes take place during the pB'_{355} to pB_{355} transition. The large positive amplitude of the spectral marker at 1624 cm^{-1} in the $pB_{355} - pG_{446}$ spectrum evidences large structural changes in the protein secondary structure. The spectral marker for the polar side chain groups with double bonds (1610−1560 cm^{-1}) exhibits four positive bands, indicating changes in the environment of four polar side chain groups. Exposed polar and charged groups are not expected to contribute to the difference spectra as long as they remain exposed. There are 12 buried and partially buried polar groups in pG_{446} (*14*). Therefore, the data indicate that the large global conformational changes during the pB'_{355} to pB_{355} transition involve one-third of the buried and partially buried groups. The molecular mechanism for PYP activation has been disputed (*13*, *27*, *29*). We present the following strong evidence for the decisive role of Glu46 ionization in driving signaling state formation.

The COO^- group of Glu46 in pB'_{355} is embedded in a highly hydrophobic environment (Figure 2). Buried charges in hydrophobic interiors of proteins exert strong destabilizing effects on protein structures (*1*, *2*). We show a method (see Materials and Methods) for estimating the electrostatic energy difference between a buried COO^- group in a highly hydrophobic environment (with a dielectric constant ϵ of 2.5) and the same group in a less hydrophobic or hydrophilic environment (ϵ of 5−7) in proteins. Using a charge q of −0.80 e and a dipole moment p of 1.00 eÅ from our ab initio Gaussian98 calculation or the larger values of q (−1.0 e) and p (1.3 eÅ) for the COO^- group, the electrostatic energy difference is found to be 28−55 kJ/mol. In comparison, a typical value for protein folding energy is approximately 40 kJ/mol (*2*). Therefore, the destabilizing electrostatic energy of this single buried COO^- group of Glu46 in pB'_{355} is sufficiently strong to drive large conformational changes during pB_{355} formation.

The electrostatic energy of a buried charge is determined by two effects (*16*): the effective radius of the charge and the effective dielectric constant of its environment (see Materials and Methods). Both effects contribute to an increased electrostatic energy upon the pG_{446} to pB'_{355} transition. The negative charge on the pCA chromophore in pG_{446} is more delocalized via conjugated electrons (larger effective radius) than the charge on the COO^- group of Glu46 in pB'_{355}. In addition, the binding pocket of the pCA (Figure 2) in pG_{446} and pR_{465} is less hydrophobic with 40% polar atoms (nine oxygens, eight nitrogens, and one sulfur) and 60% nonpolar atoms (29 carbons) than the binding pocket of the COO^- of Glu46 in pB'_{355} with 17% polar atoms (two oxygens) and 83% nonpolar atoms (11 carbons).

To experimentally investigate the role of creating a new buried charge, COO^- of Glu46, in driving large conformational changes, we performed time-resolved FTIR spectroscopy on the photocycle of the E46Q mutant, in which formation of a new buried charge (COO^-) is abolished. A pB-like state is formed during the photocycle of the E46Q mutant (*24*). This pB state was identified by visible absorption spectroscopy, which is a local probe only sensitive to the pCA chromophore, not to the entire protein. In contrast, time-resolved FTIR spectroscopy is sensitive to the structure

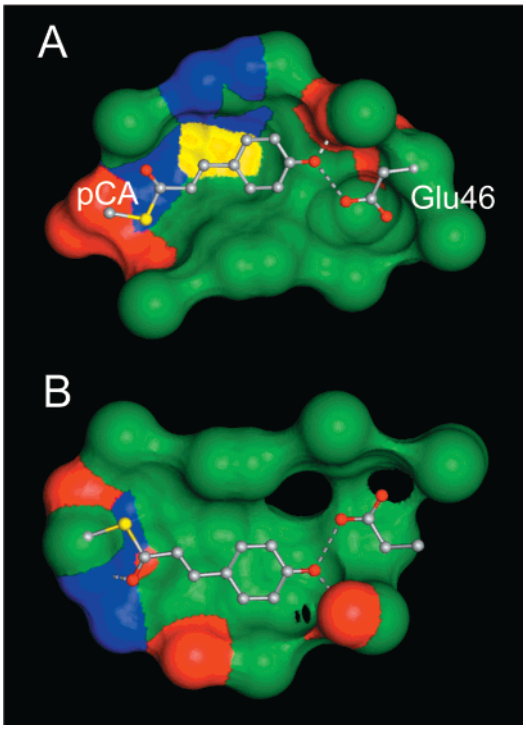

FIGURE 2: Electrostatic properties of the binding pocket for the pCA chromophore and the COOH group of Glu46 in pG_{446}. The binding pocket is formed from the atoms on the first shell, and is depicted as a surface generated using a probe with a 1.6 Å radius. The top half of the binding pocket (A) is formed, for pCA, from the atoms of Tyr42 (OH, CZ), Thr50 (OG1, CB, CG2), Arg52 (NH1, NH2, CZ, NE, CD), Tyr94 (CE2), Thr95 (O), Phe96 (C, CA, CB, CD1, CD2, CE1, CE2, CG, CZ), Asp97 (N, OD1, OD2), Tyr98 (N, CB), and Met100 (SD) and, for the carboxylic group of Glu46, from the atoms of Gly29 (CA), Glu46 (CA, O), Ile49 (CB, CD1, CG2), and Val122 (CG1). The bottom half of the binding pocket (B) is formed, for pCA, from the atoms of Ile31 (CD1), Tyr42 (OH, CZ, CE2), Phe62 (CZ, CE1), Val66 (CG1, O), Ala67 (CA, CB, O), Pro68 (N), Cys69 (CA, N, O), Thr70 (CG2, N), Tyr94 (CE2), and Phe96 (CZ, CE1) and, for the COOH group of Glu46, from the atoms of Gly29 (C, CA), Ile31 (CD1, CG1), and Val122 (CG1, CG2). The green areas (carbon) represent a low-dielectric medium, whereas red (oxygen), blue (nitrogen), and yellow (sulfur) areas denote a high-dielectric environment. The chromophore and the side chain group of Glu46 are illustrated in sticks and balls, with gray for carbon, red for oxygen, and yellow for sulfur. Three hydrogen bonds are shown as dashed lines. Since the binding pocket of the COOH group of Glu46 is very rigid in pG_{446} and the structural fold of pB'_{355} is very similar to that of pG_{446}, the binding pocket for the COO^- group of Glu46 in pB'_{355} is expected to be very similar to that in pG_{446} as illustrated here.

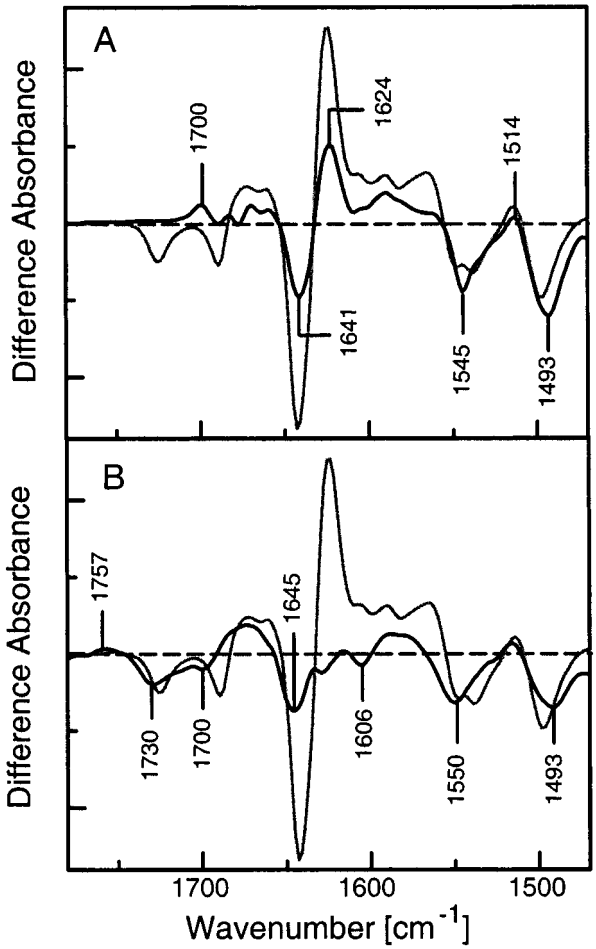

FIGURE 3: pB − pG infrared spectra of the E46Q mutant (A) (black) which shows significantly reduced amplitudes of both the amide I band and signals from side chain groups around 1689 cm^{-1} and over the 1610−1580 cm^{-1} region. (B) pB − pG infrared spectrum of PYP in $P6_3$ crystals. The pB_{355} − pG_{446} spectrum of wt-PYP in solution (gray) is presented in both panels A and B for comparison; the dashed lines represent $\Delta A = 0$.

of both the chromophore and the entire protein. The pB − pG FTIR difference spectrum of the E46Q mutant (Figure 3A) reveals that the intensities of the amide I signals, probing the backbone structural changes, are dramatically reduced in the E46Q mutant compared with that of wt-PYP, and that the strong 1689 cm^{-1} band for a side chain group in wt-PYP is not present in the E46Q mutant. Therefore, the extent of conformational changes from pG to pB is greatly reduced in the E46Q mutant. This result demonstrates that the protonation of the chromophore by itself has little effect on the protein conformation. It is the formation of a new buried charge, COO^- of Glu46, that drives large conformational changes.

Importance and Limitations of Time-Resolved X-ray Crystallography. X-ray crystallography of static proteins is the most powerful technique for resolving the three-dimensional structure of proteins in atomic detail, and has played a crucial role in understanding the molecular mechanism of protein function. Time-resolved X-ray crystallography has recently become possible (*22*, *29*), opening a novel field of investigation on the structural changes during protein function. The X-ray structure of pB was determined using millisecond time-resolved X-ray crystallography on $P6_3$ PYP crystals (*29*). The pB structure formed in $P6_3$ crystals was found to be very similar to that of pG_{446}, in contrast with other observations on pB_{355} in aqueous solution using a range of techniques (*27*, *28*). To resolve this dispute, we performed time-resolved FTIR spectroscopy on wt-PYP in $P6_3$ crystals. The pB − pG spectrum of PYP in $P6_3$ crystals (Figure 3B) reveals no changes in the protein backbone (amide I), and dramatically reduced changes in the side chain groups (1610−1560 cm^{-1}). Therefore, the structure of the putative signaling state pB_{355} is not developed in $P6_3$ crystals. Furthermore, a positive band of COOD stretching is observed at 1757 cm^{-1}, indicating the presence of protonated Glu46 in a highly hydrophobic pocket in pB in $P6_3$ crystals.

Our results demonstrate that the structure of the pB-like state in PYP $P6_3$ crystals is very different from that of the pB_{355} state in PYP solution. In addition, the pB to pG transition is approximately 10 times faster in $P6_3$ crystals

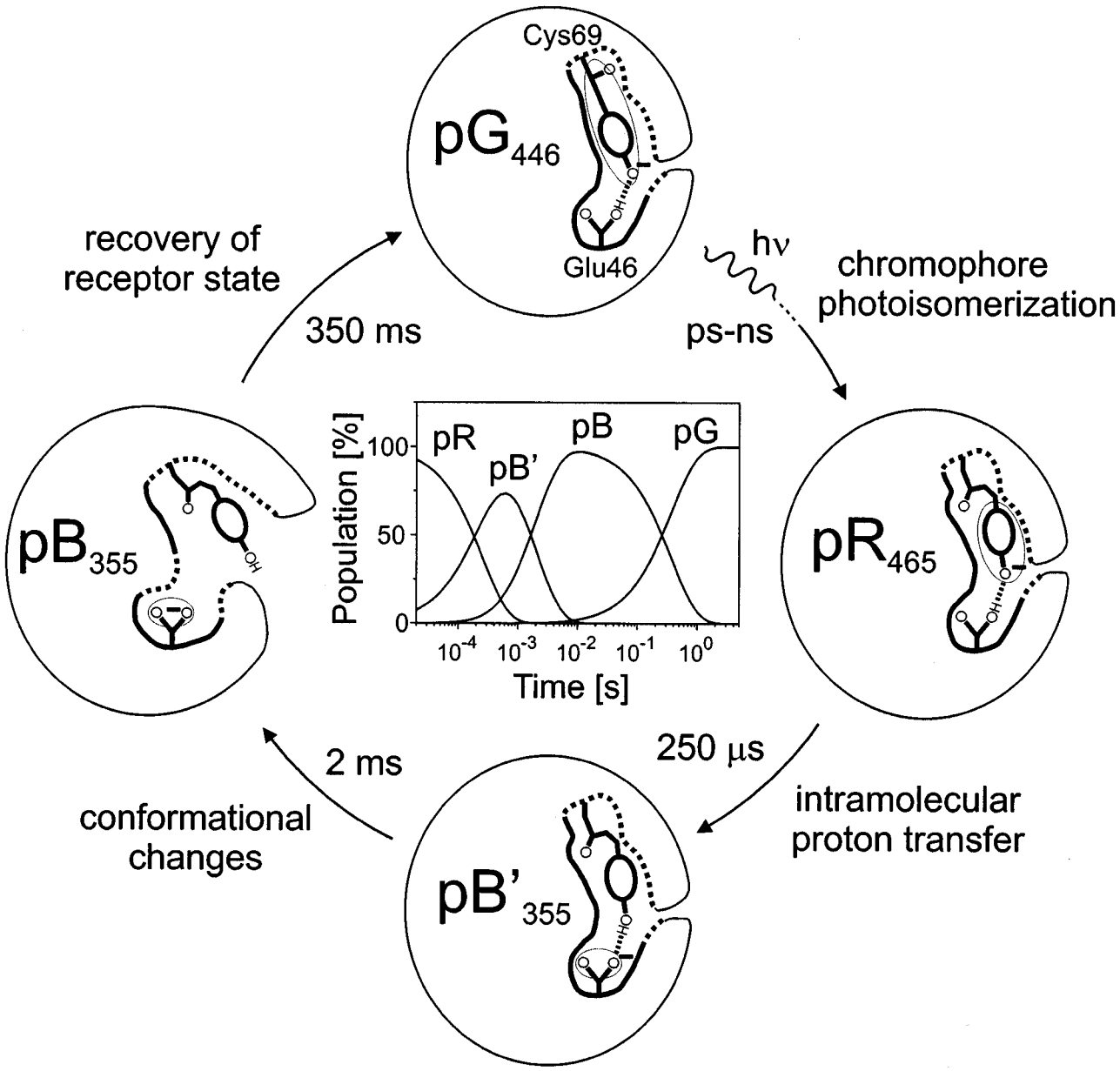

FIGURE 4: PYP photocycle and a molecular mechanism for PYP activation. Three intermediates (pR_{465}, pB'_{355}, and pB_{355}) of the PYP photocycle are depicted. Their population accumulations are shown in the inset. The electrostatic properties of the binding pocket for the chromophore and Glu46 are denoted using thick dashed lines for high-dielectric environments, thick solid lines for low-dielectric environments, and thin solid lines for unspecified dielectric environments. The charge delocalizations are qualitatively represented by shaded ovals.

than in solution, in agreement with kinetic measurement of single $P6_3$ crystals (*15*). Therefore, the photocycle of PYP is both structurally and kinetically different between the $P6_3$ crystal state and the solution state.

The large differences between the pB states in crystals and in aqueous solution raise the question of which pB state is active in intact cells. This question will be discussed here in terms of protein concentration, water content, and lattice contacts. The total protein concentration in the cytoplasm of bacteria is ~50 mg/mL. In $P6_3$ crystals, the PYP concentration is approximately 650 mg/mL. In comparison, the PYP concentration of our FTIR samples is 140 mg/mL (10 mM), and is therefore closer to physiological conditions. In terms of water content, PYP is a highly water soluble protein. PYP molecules in our FTIR samples are fully hydrated with 4800 water molecules per PYP. When the hydration level of proteins is reduced to ~350 water molecules per PYP, the large structural changes during pB formation are fully suppressed (*27*). The hydration level in $P6_3$ crystals is ~500 H_2O molecules per PYP, only slightly higher than 350 H_2O molecules per PYP. This partial dehydration can reduce the extent of structural changes in $P6_3$ crystals. Finally, the inhibition of large conformational changes may be caused by restraints imposed by the large number of protein−protein contacts that form the $P6_3$ crystal lattice (58 contacts per PYP) (*30*). In general, such lattice contacts may prevent the full development of conformational changes during the functional cycle of a protein (*31*). Therefore, the structure of pB_{355} formed in aqueous solution at room temperature and neutral pH of our FTIR samples is expected to be closer to that of the putative signaling state under physiological conditions than the pB structure formed

in crystals. It is possible, however, that interactions between PYP and its signal transducer may affect the structure of the pB state in the living cell.

We show that time-resolved FTIR spectroscopy is a powerful technique for testing the transient structures of proteins in solution and in crystals. Prior to this work, only one time-resolved FTIR spectroscopic study of protein crystals has been reported (*32*) on bacteriorhodopsin (bR), a membrane protein for the light-driven proton pump. Structural changes of bR during its proton pumping photocycle are very similar in both membrane and crystal states. Since bR molecules form two-dimensional crystals in native purple membranes, no large conformational changes are present even in the native state. It is therefore not too unexpected that the structural changes in the three-dimensional crystals of bR molecules are similar to those in the two-dimensional native crystals. In contrast, PYP is a water soluble photoreceptor protein, and large conformational changes can well be associated with signal relay via intermolecular interactions. In conclusion, one must be cautious in drawing conclusions regarding the functional mechanism of proteins based on time-resolved X-ray crystallography prior to direct experimental testing on the structural developments of a protein during its functional process in both crystal and solution states.

A Molecular Mechanism for PYP Activation. We propose the following molecular mechanism for receptor activation in PYP, as depicted in Figure 4. In the receptor state, pG_{446}, a built-in structural fault for a protein quake is present at the photoactive site, consisting of the negatively charged phenolic group of the pCA chromophore and the protonated carboxylic group of Glu46. These two groups exhibit anomalously shifted p*K*s in opposite directions. The abnormal charge state of the pCA is stabilized by intricate hydrogen bonding interactions, one counter charge from Arg52, and various hydrophilic interactions at the pCA binding pocket (*14*) (Figure 2). The neutral charge state of Glu46 is enforced by a highly hydrophobic binding pocket. In pR_{465}, chromophore photoisomerization (*13*, *33*) dramatically increases the proton affinity of the phenolic oxygen in pCA so that it abstracts a proton from Glu46 to form pB'_{355}. The origin of the enhanced proton affinity of the chromophore in pR_{465} is beyond the scope of this work. The pR_{465} to pB'_{355} transition involves localized, direct proton transfer from Glu46 to the chromophore, without changes in global protein conformation. The resulting negative charge on Glu46 is embedded in a highly hydrophobic cavity in pB'_{355}, and is therefore energetically unstable. As this charged group is searching for a more charge-friendly surrounding (higher-dielectric areas), it triggers and drives a large-amplitude protein quake. The epicenter of the protein quake is located at the hydrophobic active site where a new buried charge, COO^- of Glu46, is formed via intramolecular proton transfer to the anionic pCA chromophore. The large-amplitude protein quake takes place during the pB'_{355} to pB_{355} transition, leading to the formation of the putative signaling state pB_{355}. The actual time for a protein quake to take place in individual PYP molecules is not 2 ms, the time constant of the pB'_{355} to pB_{355} transition for an ensemble of many PYP molecules, but much faster than that, on the order of picosecond to nanosecond time scales (*34*). The decisive role of Glu46 in driving a large-amplitude protein quake and PYP activation is further supported by the fact that Glu46 is conserved within the PYP family (*35*). This mechanism for protein quakes is not restricted to PYP, but may play roles during the functioning of other receptor proteins and nonreceptor proteins that require large conformational changes.

ACKNOWLEDGMENT

We thank S. Anderson and P. A. Croonquist for the preparation of $P6_3$ PYP crystals and thank B. Nie, J. Wang, and B.-C. Lee for technical assistance. We also thank D. Rousseau and R. H. Austin for valuable comments.

SUPPORTING INFORMATION AVAILABLE

List of dielectric constants for various polar and nonpolar solvents and four figures showing the assignment of a pCA-ring vibration mode around 1500 cm^{-1}, the assignment of the 1689 cm^{-1} band to a ND-containing side chain, vibrational modes of the pCA methyl ester, and normalization of the pB − pG spectrum of the E46Q mutant. This material is available free of charge via the Internet at http://pubs.acs.org.

REFERENCES

1. Honig, B., and Nicholls, A. (1995) *Science 268*, 1144−1149.
2. Honig, B., and Yang, A.-S. (1995) *Adv. Protein Chem. 46*, 27−58.
3. Ansari, A., Berendzen, J., Bowne, S. F., Frauenfelder, H., Iben, L. E., Sauke, T. B., Shyamsunder, E., and Young, R. D. (1985) *Proc. Natl. Acad. Sci. U.S.A. 82*, 5000−5004.
4. Pellequer, J. L., Wager-Smith, K. A., Kay, S. A., and Getzoff, E. D. (1998) *Proc. Natl. Acad. Sci. U.S.A. 95*, 5884−5890.
5. Taylor, B. L., and Zhulin, I. B. (1999) *Microbiol. Mol. Biol. Rev. 63*, 479−506.
6. Meyer, T. E., Yakali, E., Cusanovich, M. A., and Tollin, G. (1987) *Biochemistry 26*, 418−423.
7. Sprenger, W. W., Hoff, W. D., Armitage, J. P., and Hellingwerf, K. J. (1993) *J. Bacteriol. 175*, 3096−3104.
8. Jiang, Z., Swem, L. R., Rushing, B. G., Devanathan, S., Tollin, G., and Bauer, C. E. (1999) *Science 285*, 406−409.
9. Hoff, W. D., Dux, P., Hard, K., Devreese, B., Nugteren-Roodzant, I. M., Crielaard, W., Boelens, R., Kaptein, R., van Beeumen, J., and Hellingwerf, K. J. (1994) *Biochemistry 33*, 13959−13962.
10. Baca, M., Borgstahl, G. E., Boissinot, M., Burke, P. M., Williams, D. R., Slater, K. A., and Getzoff, E. D. (1994) *Biochemistry 33*, 14369−14377.
11. Hoff, W. D., van Stokkum, I. H., van Ramesdonk, H. J., van Brederode, M. E., Brouwer, A. M., Fitch, J. C., Meyer, T. E., van Grondelle, R., and Hellingwerf, K. J. (1994) *Biophys. J. 67*, 1691−1705.
12. Ujj, L., Devanathan, S., Meyer, T. E., Cusanovich, M. A., Tollin, G., and Atkinson, G. H. (1998) *Biophys. J. 75*, 406−412.
13. Xie, A., Hoff, W. D., Kroon, A. R., and Hellingwerf, K. J. (1996) *Biochemistry 35*, 14671−14678.
14. Borgstahl, G. E., Williams, D. R., and Getzoff, E. D. (1995) *Biochemistry 34*, 6278−6287.
15. Ng, K., Getzoff, E. D., and Moffat, K. (1995) *Biochemistry 34*, 879−890.
16. Jackson, J. D. (1999) *Classical Electrodynamics*, 3rd ed., John Wiley & Sons, New York.
17. Hage, W., Kim, M., Frei, H., and Mathies, R. A. (1996) *J. Phys. Chem. 100*, 16026−16033.
18. Rothschild, K. J. (1992) *J. Bioenerg. Biomembr. 24*, 147−167.
19. Venyaminov, S. U., and Kalnin, N. N. (1990) *Biopolymers 30*, 1259−1271.
20. Arrondo, J. L., Muga, A., Castresana, J., and Goñi, F. M. (1993) *Prog. Biophys. Mol. Biol. 59*, 23−56.

21. Venyaminov, S. Y., and Kalnin, N. N. (1990) *Biopolymers 30*, 1243−1257.
22. Perman, B., Srajer, V., Ren, Z., Teng, T., Pradervand, C., Ursby, T., Bourgeois, D., Schotte, F., Wulff, M., Kort, R., Hellingwerf, K., and Moffat, K. (1998) *Science 279*, 1946−1950.
23. Nakanishi, K., and Solomon, P. M. (1977) *Infrared Absorption Spectroscopy*, Holden-Day, San Francisco.
24. Genick, U. K., Devanathan, S., Meyer, T. E., Canestrelli, I. L., Williams, E., Cusanovich, M. A., Tollin, G., and Getzoff, E. D. (1997) *Biochemistry 36*, 8−14.
25. Nagle, J. F., and Mille, M. (1981) *J. Chem. Phys. 74*, 1367−1372.
26. Mihara, K., Hisatomi, O., Imamoto, Y., Kataoka, M., and Tokunaga, F. (1997) *J. Biochem. 121*, 876−880.
27. Hoff, W. D., Xie, A., Van Stokkum, I. H., Tang, X. J., Gural, J., Kroon, A. R., and Hellingwerf, K. J. (1999) *Biochemistry 38*, 1009−1017.
28. Rubinstenn, G., Vuister, G. W., Mulder, F. A., Dux, P. E., Boelens, R., Hellingwerf, K. J., and Kaptein, R. (1998) *Nat. Struct. Biol. 5*, 568−570.
29. Genick, U. K., Borgstahl, G. E., Ng, K., Ren, Z., Pradervand, C., Burke, P. M., Srajer, V., Teng, T. Y., Schildkamp, W., McRee, D. E., Moffat, K., and Getzoff, E. D. (1997) *Science 275*, 1471−1475.
30. Van Aalten, D. M. F., Crielaard, W., Hellingwerf, K. J., and Joshua-Tor, L. (2000) *Protein Sci. 9*, 64−72.
31. Makinen, M. W., and Fink, A. L. (1977) *Annu. Rev. Biophys. Bioeng. 6*, 301−343.
32. Heberle, J., Buldt, G., Koglin, E., Rosenbusch, J. P., and Landau, E. M. (1998) *J. Mol. Biol. 281*, 587−592.
33. Genick, U. K., Soltis, S. M., Kuhn, P., Canestrelli, I. L., and Getzoff, E. D. (1998) *Nature 392*, 206−209.
34. Frauenfelder, H., and Wolynes, P. G. (1985) *Science 229*, 337−345.
35. Kort, R., Hoff, W. D., Van West, M., Kroon, A. R., Hoffer, S. M., Vlieg, K. H., Crielaand, W., Van Beeumen, J. J., and Hellingwerf, K. J. (1996) *EMBO J. 15*, 3209−3218.

BI002449A